Volume 146
Number 13
7 July 2021
Pages 4097-4404

Analyst

rsc.li/analyst

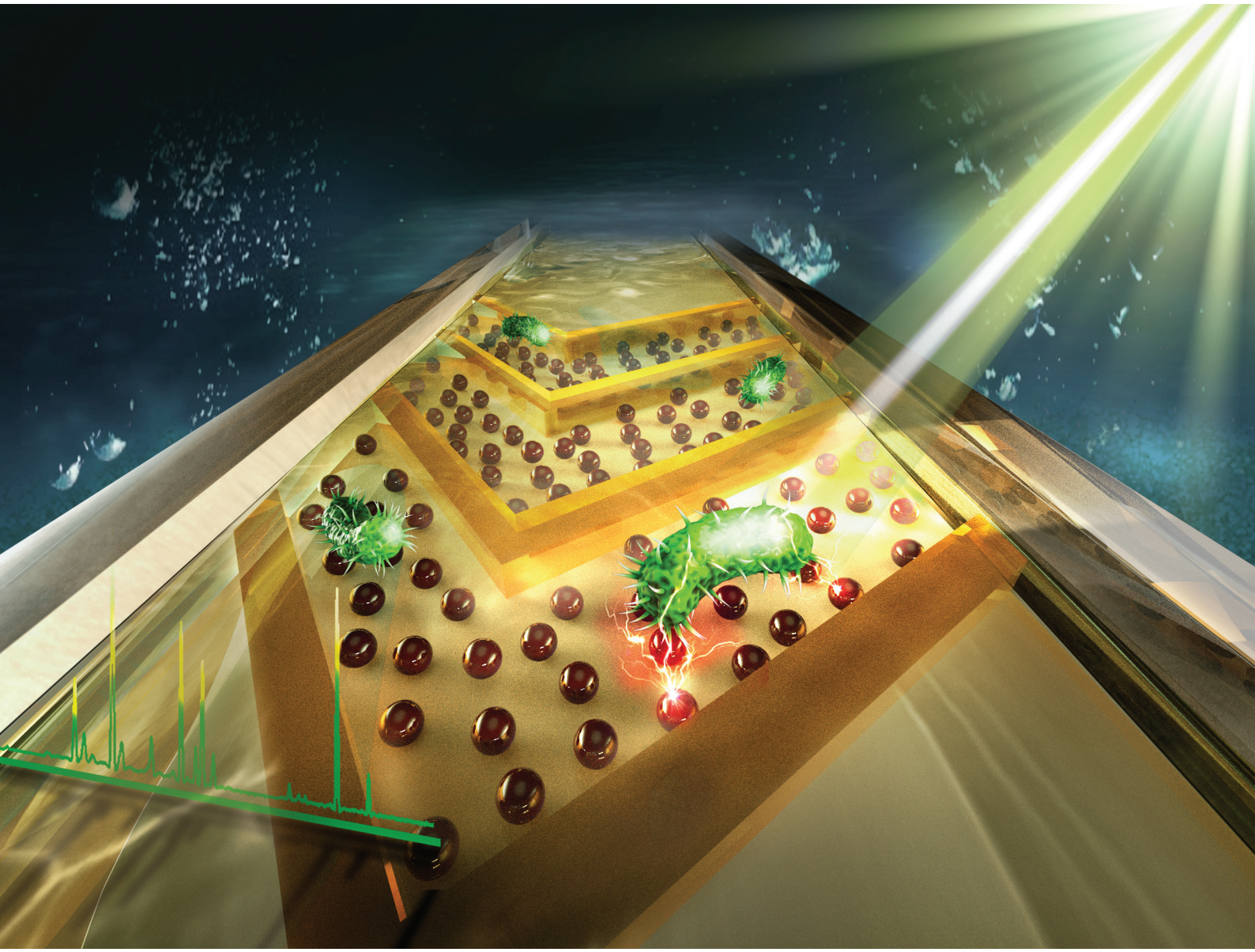

ISSN 0003-2654

ROYAL SOCIETY OF CHEMISTRY

PAPER

Minghui Song, Meicheng Yang, Liang Qiao *et al.*
Highly efficient enrichment and identification of pathogens using a herringbone microfluidic chip and by MALDI-TOF mass spectrometry

Analyst

ROYAL SOCIETY OF CHEMISTRY

PAPER

View Article Online
View Journal | View Issue

Cite this: *Analyst*, 2021, **146**, 4146

Highly efficient enrichment and identification of pathogens using a herringbone microfluidic chip and by MALDI-TOF mass spectrometry†

Yueqing Shen, ‡[a,b] Jia Yi,‡[b] Minghui Song,*[a] Dandan Li,[b] Yi Wu,[b] Yan-Jun Liu,[b] Meicheng Yang*[a] and Liang Qiao *[b]

Bacterial infections cause considerable morbidity and expensive healthcare costs. The prescription of broad-spectrum antimicrobial drugs results in failure of treatment or overtreatment and exacerbates the spread of multidrug-resistant pathogens. There is an emergent demand for rapid and accurate methods to identify pathogens and conduct personalized therapy. Here, we develop a herringbone microfluidic chip integrated with vancomycin modified magnetic beads (herringbone-VMB microchip) to enrich pathogens. The enriched pathogens are identified by matrix-assisted laser desorption ionization time-of-flight mass spectrometry. The herringbone-VMB microchip applies passive mixing of bacterial samples by generating microvortices, which significantly enhances the interaction between bacteria and vancomycin modified magnetic beads and leads to more efficient enrichment compared to in-tube extraction. Four common pathogens in urinary tract infections are utilized to validate the method, and the capture efficiency of the bacteria from urine is up to 90%. The whole procedure takes 1.5 hours from enrichment to identification. This method shows potential in shortening the turnaround time in the clinical diagnosis of bacterial infections.

Received 25th February 2021,
Accepted 18th April 2021

DOI: 10.1039/d1an00335f

rsc.li/analyst

Introduction

Bacterial infections, such as urinary tract infections (UTIs), are the most common community-acquired and hospital-acquired infections, causing considerable morbidity and medical care expenditure.[1,2] Moreover, complicating factors, such as obstructive urolithiasis, indwelling catheters and urinary tract surgeries, increase the risk of urosepsis, and the related mortality is up to 20%.[3,4] It is worth noting that the inappropriate empirical therapy by broad-spectrum antibiotics contributes to the rise of drug-resistant and multidrug-resistant pathogens, which is a significant threat to global healthcare.[5] These drive the need for rapid diagnosis of infections and accurate prescription of antibiotics.

The routine screening assays of UTIs in clinical microbiology laboratories include urine dipstick tests, microscopic urinalysis and Gram stain, which, however, suffer from poor specificity and sensitivity.[6,7] Besides, the methods cannot provide information on pathogen identities. Bacterial identification methods include typical bacterial culture identification,[8] genotype-based identification, such as fluorescence *in situ* hybridization and PCR,[9] and matrix-assisted laser desorption/ionization time-of-flight (MALDI-TOF) mass spectrometry (MS)-based biotyping.[10] Bacterial culture identification is time-consuming and of low accuracy.[11] The genotype-based methods normally require prior information of all possible urinary pathogens, limiting their widespread application.[12,13] Among the various methods, MALDI-TOF MS is a powerful tool for high-throughput bacterial identification. It performs well without prior information and is friendly to non-professional users. However, pure isolates are required for MALDI-TOF-based bacterial identification, which usually takes 6 to 48 hours or even longer, limiting the turnaround time of bacterial identification by MALDI-TOF MS.[14]

Microfluidic chip-based methods have been developed to enrich bacteria from original specimens based on mechanical isolation and biochemical affinity to shorten the turnaround time of bacterial culture.[15–18] While designing microfluidic

[a]*NMPA Key Laboratory for Testing Technology of Pharmaceutical Microbiology, Shanghai Institute for Food and Drug Control, Shanghai 201203, China. E-mail: sminghui88@163.com, yangmeicheng@vip.sina.com*
[b]*Department of Chemistry, and Institutes of Biomedical Sciences, Fudan University, Shanghai 200433, China. E-mail: liang_qiao@fudan.edu.cn*

†Electronic supplementary information (ESI) available: Supplementary figures and table. See DOI: 10.1039/d1an00335f

‡These authors contributed equally.

chips with special patterns, the interaction between target bacteria and recognition units can be enhanced by inducing microvortices in laminar flow with a low *Re*.[19] Compared with the active mixing driven by external power, passive mixing by specific micro-structures has advantages of energy saving and less heat damage, and thus passive mixers have been adopted frequently to increase the mixing efficiency in microfluidics.[20,21] Zheng *et al.* developed an optical biosensor based on porous gold@platinum nanocatalysts integrated with a passive micromixer for the detection of *Salmonella typhimurium*.[22] Jung *et al.* reported a passive micromixer combined with capillary electrophoresis for pathogen detection.[23]

In addition to the microfluidic chips based on polydimethylsiloxane (PDMS), paper-based chips relying on biochemical affinity have also been widely used to isolate bacteria from complex matrices. Wang *et al.* deposited antibody-conjugated gold nanoparticles on a graphene oxide paper-based working electrode to capture and detect *Escherichia coli* O157:H7 from both ground beef and cucumber.[24] Pang *et al.* developed a paper-based enzyme-linked immunosorbent assay to detect *E. coli* O157:H7 from Chinese cabbage.[17]

A variety of materials with different recognition units have been reported for bacterial capture. Zheng *et al.* fabricated a lectin functionalized ZnO nanorod for *Escherichia coli* capture and detection.[25] Liu *et al.* developed three-dimensional carbon foam pre-grafted with nanowires to capture bacteria from blood, adopting concanavalin A as the recognition unit.[26] Choi *et al.* prepared gold nanoparticles modified with specific antibodies to capture *Salmonella enterica*.[27] Shen *et al.* developed a bacterial capture platform based on mesoporous TiO_2-coated magnetic nanoparticles modified with a target aptamer.[28] The adoption of specific recognition units, such as antibodies, aptamers, peptides, and bacteriophages, can provide high sensitivity against target pathogens, but less flexibility in application. For untargeted analysis by MALDI-TOF, recognition units against a broad range of pathogens, such as concanavalin A,[26,29] Fc-mannose-binding lectin,[30] 4-MPBA,[31] and vancomycin,[32] are preferred. It is worth mentioning that vancomycin has been proven to be a powerful broad-spectrum recognition unit of Gram-positive pathogens with relatively high capture efficiency in a number of reports.[32–34]

Herein, we report a herringbone microfluidic chip combined with vancomycin modified magnetic beads (herringbone-VMB microchip) to enrich bacteria followed by MALDI-TOF identification. With the herringbone microstructure, chaotic mixing occurs in the microfluidic chip that can improve the contact probability between bacteria in fluid and immobilized magnetic beads for more efficient bacterial enrichment. Four UTI pathogens were used to validate the performance of the herringbone-VMB microchip. Highly efficient enrichment of target bacteria from urine samples was obtained. The enriched bacteria were then subjected to MALDI-TOF MS analysis. The whole analysis procedure takes 1.5 hours from enrichment to identification, and it is feasible to identify pathogens directly from UTI patients without bacterial culture.

Experimental section

Reagents and chemicals

Vancomycin hydrochloride (from *Streptomyces orientalis*, ≥90%), 4-morpholineethanesulfonic acid (MES, ≥99%), *N*-(3-dimethylaminopropyl)-*N*′-ethylcarbodiimide hydrochloride (EDC, ≥98.0%), *N*-hydroxysuccinimide (NHS, 98%), 2,5-dihydroxy-benzonic acid (DHB, >99.0%), Tween-20 and alpha-Cyano-4-hydroxycinnamic acid (HCCA, ≥99%) were all from Sigma-Aldrich Inc. (Saint Louis, USA). PuriMag™ GL-NH_2 magnetic beads (10 mg mL^{-1}, 200 nm in diameter) were from PuriMag Biotech Ltd (Xiamen, China). Phosphate buffered saline (PBS) was from Sangon Biotech Co., Ltd (Shanghai, China). A MICROCHEM SU-8 2025 Photoresist and MICROCHEM SU-8 Developer were from Kayaku Advanced Materials, Inc. (MA, USA). Acetonitrile (ACN, ≥99.9%) was purchased from Merck (Darmstadt, Germany). Trifluoroacetic acid (TFA, 99.0%) was from Adamas Reagent Co., Ltd (Shanghai, China). The SYLGARD 184 silicone elastomer base and curing agent were from Dow Corning Corp (MI, USA). Deionized (DI) water (18.2 MΩ cm) was purified using a Smart-Q deionized water system (Hitech Instruments Co., Ltd, Shanghai, China) and used in all aqueous solutions.

Design and fabrication of the microfluidic chip

The microfluidic chip was composed of repetitive herringbone units and a serpentine channel (Fig. 1A) to induce micro-vortices in a laminar flow. The dimension of the designed microfluidic chip was 82.0 mm × 57.2 mm (Fig. S1†). The width and the depth of the microchannel were 1000 μm and 100 μm, respectively, while the height of each embedded herringbone ridge was 50 μm. A pattern of ten herringbones was arranged periodically asymmetric, two such patterns form a unit, and there were 221 herringbone units (Fig. S1 and 2†).

The fabrication of the mold of the microfluidic chip was based on an alignment method employing a multilayer soft-lithography technology.[35] The mask of each layer was first designed and a multilayer mold was prepared by stacking two patterned layers on a silicon wafer (Fig. S1†). Then the PDMS layers with and without patterns were fabricated by pouring a fully blended mixture of the base and curing agent (weight ratio = 10 : 1) into the mold with subsequent baking at 65 °C for 2 hours. Then, the two PDMS layers were peeled off gently and punched to create an inlet and an outlet. The processed PDMS layers were assembled by the oxygen plasma bonding method[36] and thermally stabilized at 65 °C for 2 hours for strong crosslinking.

Simulation of fluid flow in microchannels

The simulation of fluid flow in microchannels was powered using the Fluent module in Ansys 19.2 (Southpointe 2600

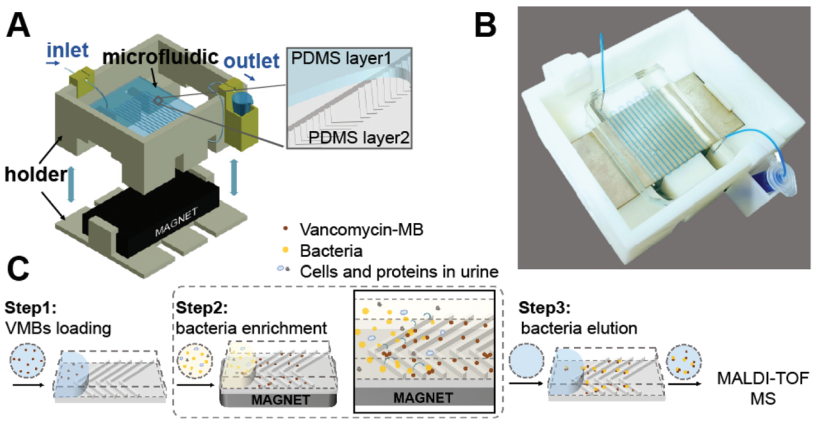

Fig. 1 (A) Schematic illustration of the assembly of the integrated device for bacterial capture, consisting of a magnet, a herringbone microchip and a 3D-printed base. Fluids containing bacteria are pumped into the microfluidic chip from the inlet and collected at the outlet with a clean microcentrifuge tube. (B) Photo of the integrated device. (C) Workflow of enrichment and MALDI-TOF analysis of UTI bacteria, consisting of the loading of vancomycin modified magnetic beads (VMBs), enrichment of bacteria from urine, elution of VMB@bacteria, and MALDI-TOF MS analysis.

Ansys Drive, Canonsburg, USA). Since the chip was made up of 221 repetitive units, we chose one unit (3.88 mm × 1.0 mm × 0.1 mm) as the simulation object. The input flow rate was 500 μL h^{-1} (*i.e.*, the inlet velocity = 0.001389 m s^{-1}), and the outlet flow rate was dependent on ambient pressure. The fluid was set as water and simulated under the Laminar-viscous model. The global parameters were set corresponding to the actual experimental conditions: the gravitational acceleration, pressure and temperature were 9.81 m s^{-2}, 101.325 kPa and 288.16 K, respectively.

Modification of vancomycin on the magnetic beads

The synthesis of vancomycin modified magnetic beads (VMBs) was performed using an EDC/NHS crosslinking method modified from a previous report.[32] One hundred μL of GL-NH_2 magnetic beads (10 mg mL^{-1}) were extracted and washed with 100 μL of MEST (30 mmol L^{-1} MES, 0.05% Tween-20 in DI water, pH = 6.0) 3 times. Then the magnetic beads were resuspended in 200 μL of MEST solution containing 10 mg of EDC, 10 mg of NHS, and 20 mg of vancomycin, followed by an ultrasonic reaction for 1 hour. After the reaction, the supernatant was removed from the VMBs by employing a magnetic separator and the VMBs were washed with 200 μL of MEST 4 times to remove the unreacted vancomycin. Finally, the VMBs were resuspended in 200 μL of MEST solution, *i.e.* with a final concentration of 5 mg mL^{-1} VMBs, and stored at 4 °C for use (≤13 days, Fig. S3†).

Bacterial culture

Four Gram-positive strains highly related to UTIs were involved in this work, including *Staphylococcus aureus* (*S. aureus* strain ATCC 25923), *Staphylococcus hominis* (*S. hominis* strain R16932), *Streptococcus epidermidis* (*S. epidermidis* strain CICC 10436), and *Enterococcus gallinarum* (*E. gallinarum* strain W19007). The strains were obtained from the American Type Culture Collection (ATCC, Manassas, VA, USA), China Center of Industrial Culture Collection (CICC, Beijing, China), or Bioyong Technologies Inc. (Beijing, China). These strains were cultivated in TSB (Trypticase Soy Broth) overnight at 37 °C in a shaking incubator at 175 rpm. Then 1 mL of the cultures was centrifuged at 12 000*g* for 2 min, washed 3 times, and finally diluted in PBST (PBS buffer with 0.05% Tween-20) to prepare the bacterial suspension for further use. To quantify the numbers of bacteria, the bacterial concentration–absorbance curve was plotted for each bacterial strain at a wavelength of 450 nm (OD_{450}) using a Multiskan FC spectrophotometer (Thermo, Massachusetts, USA) (Fig. S4†).

Assembly of the microfluidic setup

The VMB suspension was pumped into the microfluidic chip to fill up the microchannels and then a 3D-printed substrate implanted with a NdFeB block magnet was posed under the chip to immobilize the VMBs and remove the buffer (Fig. 1A). After the MEST buffer was flushed out of the microfluidic chip at a flow rate of 2500 μL h^{-1} (controlled by LSP04-1A 4 Channels Syringe Pump, Longer Precision Pump Co., Ltd, China), the VMBs were evenly dispersed and tightly attached on the bottom of the herringbone microstructures for bacterial enrichment (Fig. S5†).

Extraction of bacteria

Bacterial sample (10^7 CFU mL^{-1} bacteria in PBST, 250 μL) was pumped into the microfluidic device at a flow rate of 250 μL h^{-1}. After each enrichment experiment, the magnet was removed and the bacteria@VMB complex was flushed off the channels and washed with DI water three times to form 1 μL of the bacteria@VMB extraction sample for the subsequent MALDI-TOF identification. The same experimental procedure was applied to extract bacteria from a spiked urine sample. 2.5 mL of human urine sample spiked with bacteria (10^6, 10^5,

10^4, or 10^3 CFU mL^{-1}) were filtered using a 5 μm filter membrane, centrifuged at 12 000*g* for 2 min, and then resuspended in 250 μL of PBST for bacterial enrichment.

The capture efficiency (η) was calculated based the OD_{450} values of the initial bacterial sample, the unbound bacterial outflow and the bacterial concentration–absorbance curve (Fig. S4†):

$$\eta = \frac{(c_0 - c)V}{c_0 V} \times 100\% = \frac{c_0 - c}{c_0} \times 100\%$$

where c_0 means the original bacterial concentration before capture, c means the bacterial concentration after capture, and V means the volume of the bacterial suspension.

MALDI-TOF identification of captured bacteria

One μL of the VMB@bacteria complex and 1 μL of the reference sample (10^8 CFU mL^{-1} bacteria in DI water) were deposited on a sample well of a MALDI plate, respectively, using a droplet-by-droplet protocol,[37] and then overlayered with 1 μL of the HCCA matrix (saturated HCCA in $V_{acetonitile}/V_{water}/V_{TFA}$ = 50% : 47.5% : 2.5%). When the solvent was completely evaporated, the samples were analysed with a MALDI-TOF mass spectrometer (Clin-TOF II, Bioyong Technologies Inc., Beijing, China) in a linear positive mode. Mass calibration was conducted with the standard protein mixture of cytochrome c, myoglobin, insulin, and ubiquitin, and the tolerance was set as 500 ppm. Five hundred laser shots were accumulated for each sample spot.

Ethics declarations

Human urine samples were collected from a healthy volunteer. The research protocol was approved by the Ethics Committee of the Fudan University, and complied with all relevant laws and regulations of China. Informed content was obtained from the participant.

Results and discussion

Simulation of the flow in the microfluidic chip

The schematic illustration of the method is shown in Fig. 1, consisting of the assembly of the experimental setup and the enrichment of bacteria for MALDI-TOF MS analysis. The herringbone microchip was designed to facilitate the uniform dispersion of VMBs and to generate chaotic mixing in microchannels. The staggered herringbone structure was originally introduced by Stroock *et al.*[19] to generate chaotic flows, which was then adopted and improved in other studies for highly efficient mixing.[38–40] The herringbone microchip used here was designed based on the basic staggered herringbones combined with a serpentine channel that can further increase the mixing efficiency.[41]

Simulation of fluid flowing through one unit of the herringbone structure was performed to evaluate the feasibility of the proposed device in inducing chaotic mixing and improving the contact probability between bacteria in fluid and immobilized VMBs. A comparison was accomplished between two types of straight microchannels containing herringbones or no herringbones. From the top view (Fig. 2A and B), typical laminar flow is observed in the channel without herringbones, where streamlines are straight with no transverse or lateral components. In contrast, the alteration of the flow direction and velocity by herringbones in the horizontal direction is clearly observed, including diverse small flows varying in velocity and direction within the fluid. The results indicate that the herringbone structure has a significant impact on the velocity and direction of streams. To further investigate the behaviour of microfluidics, both the streamline and vector plots of three representative clips in one unit of the microchannel with herringbones are shown in Fig. 2C. Information of the velocity distribution and direction change can be clearly readout. The choice of the clips depends on different observative intentions. Clip 1 and clip 2 can respectively present the effect from unilateral and bilateral herringbones, while clip 3 can reveal the fluid behaviour on the side face. In the three clips, vectors pointing toward different directions indicate that the streams can cross over each other. The streamline colour along repetitive herringbones visualizes the herringbones' function of generating transverse and lateral components within the fluid in the vertical direction. A progressive increase in velocity can be observed in streamline plots of both clip 1 and clip 2, implying the accumulating effect of herringbones in fostering the chaotic mixing and the rationality and ascendancy of using repeat herringbone units. Based on the above-demonstrated herringbone's ability in generating chaotic mixing, it is considered to enhance the contact probability between bacteria and VMBs, thus promoting their binding efficiency.

Optimization of the dosage of VMBs and the flow rate

Gram-positive and Gram-negative bacteria have different cell wall structures and components.[42] The cell wall of Gram-positive bacteria is a thick layer of peptidoglycan lying outside the plasma membrane, while that of Gram-negative bacteria consists of an outer membrane and a thin layer of intermittently cross-linked peptidoglycan network. Several affinity probes have been utilized in the capture of Gram-negative bacteria, such as lipopolysaccharide-specific aptamers,[43] anti-lipopolysaccharide antibodies,[44] and polymyxin B,[45] which show high affinity to the components of the outer membrane of bacteria. To capture Gram-positive pathogens, a high affinity to the peptidoglycan is significant. Peptidoglycan-binding protein[46] and vancomycin[32] have been reported as capture probes for Gram-positive bacteria. To capture both Gram-positive and Gram-negative bacteria, combining the two different recognition units can be a choice. Besides, probes targeting the common components of Gram-positive and Gram-negative bacteria can be selected, and there are several lectins reported for broad-spectrum capture of bacteria.[29,30]

Vancomycin is adopted in this work, which is a kind of glycopeptide antibiotic that can interact with many different

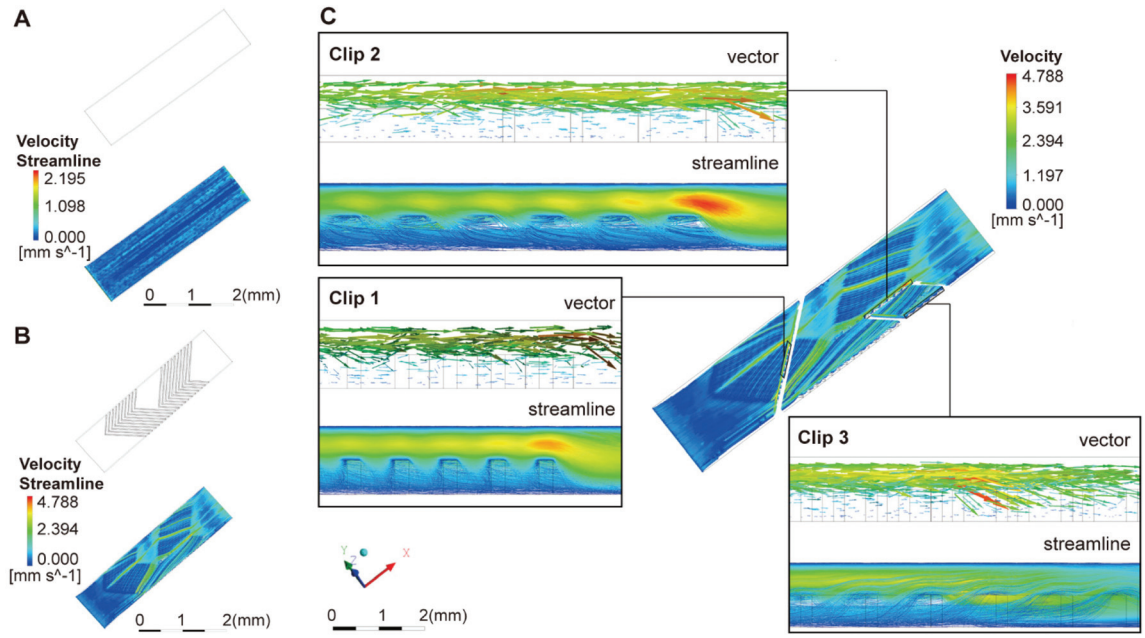

Fig. 2 Simulation of flow in the microfluidic chip. The flow field morphology observed from (A) a straight microchannel without herringbones, (B) a straight microchannel with herringbones, and (C) three clips on the microchannel with herringbones including the streamline and vector plots.

Gram-positive bacteria.[47,48] Five hydrogen bonds can form between the heptapeptide backbone of vancomycin and the D-alanyl-D-alanine on the bacterial cell wall.[47,48] To optimize the overall bacterial capture efficiency η, a series of experiments were conducted with various dosages of VMBs and different sample injection flow rates. To obtain high capture efficiency, –COOH of vancomycin was adopted to bind covalently to $-NH_2$ of GL-NH_2 magnetic beads.[32] The size and appearance of magnetic beads varied little before and after the modification of vancomycin (Fig. S6A and B†). The binding between different bacterial species and vancomycin was demonstrated by SEM images (Fig. S6C–F†).

The capture efficiency of *S. aureus* (10^7 CFU mL^{-1} in PBST) against the dosage and the flow rate is illustrated in Fig. 3A and B. The capture efficiency continuously increased with an increase of VMB dosage under 200 μg. A VMB dosage larger than 200 μg could not further enhance the capture efficiency significantly. The maximum capture efficiency was observed at a flow rate of 250 μL h^{-1}. A larger flow rate would lead to decreased capture efficiency, and a plausible explanation for this involves the binding-dissociation equilibrium. When the flow rate was high, the equilibrium cannot be reached due to insufficient binding time. Therefore, the optimal VMB dosage and optimal sample injection rate were 200 μg and 250 μL h^{-1}, respectively.

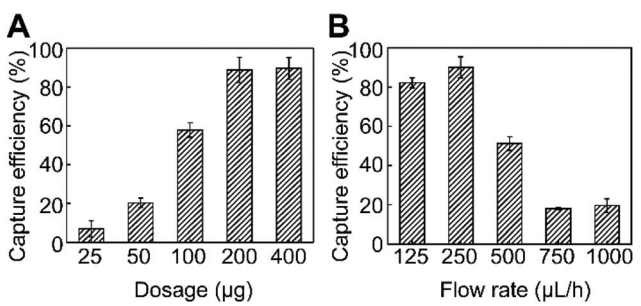

Fig. 3 Optimization of the dosage of VMBs and the flow rate of sample injection. (A) Capture efficiency with different dosages of VMBs at a flow rate of 250 μL h^{-1}. (B) Capture efficiency at different flow rates with 200 μg of VMBs. The bacterial sample was *S. aureus* in PBST (10^7 CFU mL^{-1}, 250 μL).

Enrichment and identification of bacteria from urine samples

With the optimized experimental conditions, the capture efficiency of bacteria from PBST and urine using the microfluidic device was assessed. Four common Gram-positive UTI pathogens,[49–52] *i.e. S. aureus*, *S. hominis*, *S. epidermidis* and *E. gallinarum*, were chosen to validate the performance of the method. The capture efficiencies of the four common UTI pathogens in PBST were all above ~50%, and the highest capture efficiency was up to ~90% (Table 1). As shown in Fig. 4, the mass spectra of VMBs extracted bacteria (VMB@bacteria) were similar to those of the reference bacteria. All the bacteria captured from PBST were identified correctly with a high confidence level using a Clin-TOF II MALDI-TOF MS system using a built-in bacterial spectral database (Table 1). The mass spectrum of pure VMBs (Fig. S7†) showed only two weak peaks corresponding to the double-charged and triple-charged vancomycin within the *m*/*z* range of 2500–11000, indicating that there is no significant interference from the VMBs to the characterization of captured bacteria.

Table 1 Capture efficiency and identification results of bacteria in PBST and urine samples by the herringbone-VMB microchip coupled MALDI-TOF MS

Sample	Capture efficiency (%)	Identified strain	Identification score[d]	Confidence level
S. aureus in PBST[a]	90 ± 5 [c]	*S. aureus*	55.7	High
S. aureus in urine[b]	91 ± 4 [c]	*S. aureus*	53.8	High
S. hominis in PBST [a]	90 ± 2 [c]	*S. hominis*	36.8	High
S. hominis in urine[b]	83 ± 3 [c]	*S. hominis*	29.4	High
E. gallinarum in PBST[a]	67 ± 4 [c]	*E. gallinarum*	37.3	High
E. gallinarum in urine[b]	32 ± 1 [c]	*E. gallinarum*	47.4	High
S. epidermidis in PBST[a]	50 ± 7 [c]	*S. epidermidis*	45.7	High
S. epidermidis in urine[b]	51 ± 5 [c]	*S. epidermidis*	30.3	High

[a] 10^7 CFU mL^{-1} bacteria in PBST, 250 μL. [b] 10^6 CFU mL^{-1} bacteria in urine, 2.5 mL. [c] Mean ± standard deviation, n = 3. [d] The identification score is from the Clin-TOF II MALDI-TOF MS system. According to the manufacturer's interpretation criteria, a score larger than 25 indicates highly confident identification.

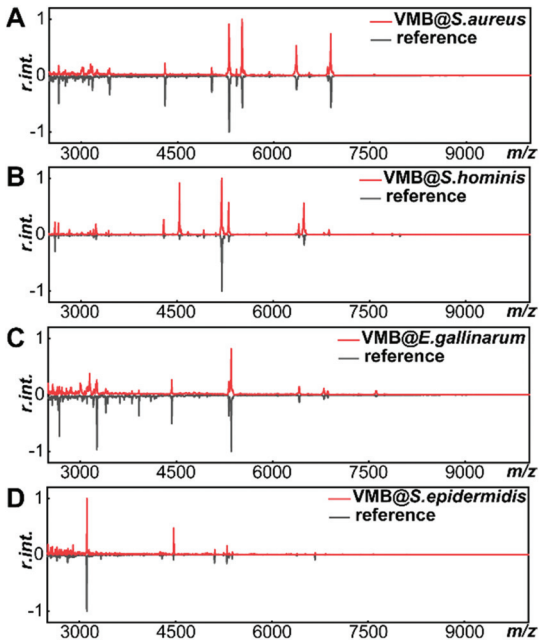

Fig. 4 MALDI-TOF mass spectra of the VMB@bacteria after the herringbone-VMB microchip extraction of bacteria from PBST samples (10^7 CFU mL^{-1}, 250 μL) compared to the reference spectra of the pure isolates of the corresponding strain. (A) *S. aureus*, (B) *S. hominis*, (C) *E. gallinarum*, and (D) *S. epidermidis*.

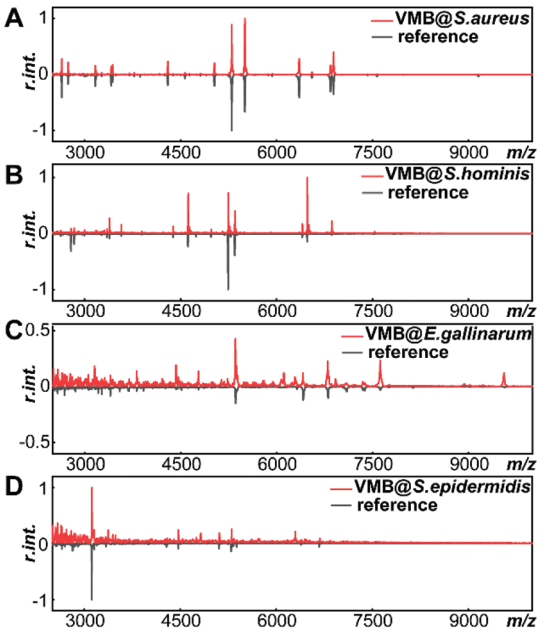

Fig. 5 MALDI-TOF mass spectra of the VMB@bacteria after the herringbone-VMB microchip extraction of bacteria from urine samples (10^6 CFU mL^{-1}, 2.5 mL) compared to the reference spectra of the pure isolates of the corresponding strain. (A) *S. aureus*, (B) *S. hominis*, (C) *E. gallinarum*, and (D) *S. epidermidis*.

We have further spiked four pathogens into the urine from a healthy volunteer at a concentration of 10^6 CFU mL^{-1}. The concentration is in accordance with the approximate bacterial concentration in UTI patients.[53] 2.5 mL of the spiked urine sample was firstly subjected to simple pretreatment, *e.g.* filtration and centrifugation, and then recovered in 250 μL of PBST for bacterial enrichment using a herringbone-VMB microchip. As shown in Table 1, the recovery of the pathogens from urine was not significantly decreased compared to that from PBST. MALDI-TOF analysis of the captured bacteria gave correct identification with high confidence as shown in Table 1 and Fig. 5. The detection limits for the four pathogens in urine were investigated, and were found to be 10^4 CFU mL^{-1} (*S. aureus*), 10^4 CFU mL^{-1} (*S. hominis*), 10^5 CFU mL^{-1} (*E. gallinarum*), and 10^4 CFU mL^{-1} (*S. epidermidis*), which was mainly limited by MALDI-TOF MS, Fig. S8.† The result indicates that the method has a potential application in the diagnosis of Gram-positive UTI pathogens.

To demonstrate the superiority of the herringbone-VMB microchip, we have also performed the capture of the pathogens using the VMBs in a centrifuge tube after optimization of the experimental conditions, such as the amount of VMBs, incubation time, and washing conditions. Compared to the results of the on-chip enrichment of two strains (*i.e.*, *E. gallinarum* and *S. epidermidis*) in urine, the capture efficiency of the in-tube enrichment was slightly lower

(Table S1†), and the quality of the mass spectra of VMB@bacteria after the in-tube enrichment was poorer (Fig. S9†). The two strains were not correctly identified due to the poor quality of the mass spectra, especially because of the interference peaks from urine (Table S1†). Intact cells, cell debris, and particles in urine samples can interfere with the identification of bacteria[54,55] and attach to the surface of the magnetic beads, thus accelerating the settlement of magnetic beads by gravity during the in-tube enrichment to decrease the utilization efficiency of the VMBs. The interference issue was largely avoided by chaotic mixing in the microchannels. In the microchip, the VMBs were pre-loaded and well dispersed by chaotic mixing (Fig. S5†), without the gravity settlement issue during the in-tube enrichment. For bacterial capture, the interaction between the bacteria and VMBs was also strengthened by chaotic mixing, instead of being limited by the diffusion in in-tube enrichment.

Conclusions

In conclusion, we have developed a new pathogen-capture microfluidic platform for MALDI-TOF MS analysis that combines the highly efficient enrichment based on the interaction between Gram-positive bacteria and vancomycin modified magnetic beads and the chaotic mixing induced by the herringbone microstructures. The resulting synergistic effects led to highly efficient enrichment and high-quality identification of pathogens spiked in urine samples. The whole procedure takes 1.5 hours from enrichment to identification, and it is feasible to identify pathogens directly from UTI patients without bacterial culture. To further shorten the assay time, parallel operation in several identical devices, decreasing the volume of sample suspension, and increasing the flow rate can be adopted. The herringbone-VMB microchip is also flexible to integrate with other bacterial characterization methods, such as Raman, fluorescence and electrochemical detection. In addition to the urine samples, the herringbone-VMB microchip can also be applied extensively in food contaminant analysis and other biofluid analysis. Future developments would include other affinity probe modified magnetic beads in the microfluidic platform to extract a broad range of pathogens, including both Gram-positive and Gram-negative bacteria, as well as fungi.

Author contributions

Yueqing Shen: formal analysis, investigation, methodology and writing. Jia Yi: conceptualization, investigation, methodology and writing. Minghui Song: conceptualization, funding acquisition and resources. Dandan Li: writing. Yi Wu: resources. Yanjun Liu: resources. Meicheng Yang: conceptualization, funding acquisition and resources. Liang Qiao: conceptualization, supervision, funding acquisition and writing.

Conflicts of interest

There are no conflicts of interest to declare.

Acknowledgements

This work was supported by the grants from the Ministry of Science and Technology of China (National Key R&D Program China, 2018YFC1603900), the National Natural Science Foundation of China (NSFC, 22022401 and 22074022), the Science and Technology Commission of Shanghai Municipality (19DZ22022600 and 18441901000) and the Open Fund Project of NMPA Key Laboratory for Testing Technology of Pharmaceutical Microbiology (2020-WSW-01).

Notes and references

1 B. Foxman, *Nat. Rev. Urol.*, 2010, **7**, 653–660.
2 T. L. Griebling, *J. Urol.*, 2005, **173**, 1281–1287.
3 F. M. E. Wagenlehner, C. Lichtenstern, C. Rolfes, K. Mayer, F. Uhle, W. Weidner and M. A. Weigand, *Int. J. Urol.*, 2013, **20**, 963–970.
4 L. E. Nicolle, *Crit. Care Clin.*, 2013, **29**, 699–715.
5 J. Wang, B. Foxman, L. Mody and E. S. Snitkin, *Proc. Natl. Acad. Sci. U. S. A.*, 2017, **114**, 10467–10472.
6 M. L. Wilson and L. Gaido, *Clin. Infect. Dis.*, 2004, **38**, 1150–1158.
7 R. D. McNair, S. R. MacDonald, S. L. Dooley and L. R. Peterson, *Am. J. Obstet. Gynecol.*, 2000, **182**, 1076–1079.
8 P. Houpikian and D. Raoult, *Emerging Infect. Dis.*, 2002, **8**, 122–131.
9 V. A. J. Kempf, K. Trebesius and I. B. Autenrieth, *J. Clin. Microbiol.*, 2000, **38**, 830–838.
10 N. Singhal, M. Kumar, P. K. Kanaujia and J. S. Virdi, *Front. Microbiol.*, 2015, **6**, 791.
11 M. Davenport, K. E. Mach, L. M. D. Shortliffe, N. Banaei, T.-H. Wang and J. C. Liao, *Nat. Rev. Urol.*, 2017, **14**, 296–310.
12 Q. Wu, Y. Li, M. Wang, X. P. Pan and Y. F. Tang, *J. Microbiol. Methods*, 2010, **83**, 175–178.
13 S. Angeletti, *J. Microbiol. Methods*, 2017, **138**, 20–29.
14 A. Freiwald and S. Sauer, *Nat. Protoc.*, 2009, **4**, 732–742.
15 A. O. Olanrewaju, A. Ng, P. DeCorwin-Martin, A. Robillard and D. Juncker, *Anal. Chem.*, 2017, **89**, 6846–6853.
16 D. Zhang, H. Bi, B. Liu and L. Qao, *Anal. Chem.*, 2018, **90**, 5512–5520.
17 B. Pang, C. Zhao, L. Li, X. Song, K. Xu, J. Wang, Y. Liu, K. Fu, H. Bao, D. Song, X. Meng, X. Qu, Z. Zhang and J. Li, *Anal. Biochem.*, 2018, **542**, 58–62.
18 X. Cui, J. Hu, J. R. Choi, Y. Huang, X. Wang, T. J. Lu and F. Xu, *Anal. Chim. Acta*, 2016, **935**, 207–212.
19 A. D. Stroock, S. K. W. Dertinger, A. Ajdari, I. Mezic, H. A. Stone and G. M. Whitesides, *Science*, 2002, **295**, 647–651.

20 C. Y. Lee, W.-T. Wang, C.-C. Liu and L. M. Fu, *Chem. Eng. J.*, 2016, **288**, 146–160.
21 C.-Y. Lee, C.-L. Chang, Y.-N. Wang and L.-M. Fu, *Int. J. Mol. Sci.*, 2011, **12**, 3263–3287.
22 L. Zheng, G. Cai, W. Qi, S. Wang, M. Wang and J. Lin, *ACS Sens.*, 2020, **5**, 65–72.
23 J. H. Jung, G.-Y. Kim and T. S. Seo, *Lab-on-a-Chip*, 2011, **11**, 3465–3470.
24 Y. Wang, J. Ping, Z. Ye, J. Wu and Y. Ying, *Biosens. Bioelectron.*, 2013, **49**, 492–498.
25 L. Zheng, Y. Wan, P. Qi, Y. Sun, D. Zhang and L. Yu, *Talanta*, 2017, **167**, 600–606.
26 L. Liu, S. Chen, Z. Xue, Z. Zhang, X. Qiao, Z. Nie, D. Han, J. Wang and T. Wang, *Nat. Commun.*, 2018, **9**, 444.
27 J. R. Choi, A. Nilghaz, L. Chen, K. C. Chou and X. Lu, *Sens. Actuators, B*, 2018, **260**, 1043–1051.
28 H. Shen, J. Wang, H. Liu, Z. Li, F. Jiang, F.-B. Wang and Q. Yuan, *ACS Appl. Mater. Interfaces*, 2016, **8**, 19371–19378.
29 Y.-Q. Li, B. Zhu, Y. Li, W. R. Leow, R. Goh, B. Ma, E. Fong, M. Tang and X. Chen, *Angew. Chem., Int. Ed.*, 2014, **53**, 5837–5841.
30 B. T. Seiler, M. Cartwright, A. L. M. Dinis, S. Duffy, P. Lombardo, D. Cartwright, E. H. Super, J. Lanzaro, K. Dugas, M. Super and D. E. Ingber, *F1000Research*, 2019, **8**, 108.
31 H. Wang, Y. Zhou, X. Jiang, B. Sun, Y. Zhu, H. Wang, Y. Su and Y. He, *Angew. Chem., Int. Ed.*, 2015, **54**, 5132–5136.
32 A. J. Kell, G. Stewart, S. Ryan, R. Peytavi, M. Boissinot, A. Huletsky, M. G. Bergeron and B. Simard, *ACS Nano*, 2008, **2**, 1777–1788.
33 M. Zhu, W. Liu, H. Liu, Y. Liao, J. Wei, X. Zhou and D. Xing, *ACS Appl. Mater. Interfaces*, 2015, **7**, 12873–12881.
34 X. Meng, G. Yang, F. Li, T. Liang, W. Lai and H. Xu, *ACS Appl. Mater. Interfaces*, 2017, **9**, 21464–21472.
35 G. M. Whitesides, E. Ostuni, S. Takayama, X. Y. Jiang and D. E. Ingber, *Annu. Rev. Biomed. Eng.*, 2001, **3**, 335–373.
36 S. Bhattacharya, A. Datta, J. M. Berg and S. Gangopadhyay, *J. Microelectromech. Syst.*, 2005, **14**, 590–597.
37 Y. Zhu, L. Qiao, M. Prudent, A. Bondarenko, N. Gasilova, S. B. Möller, N. Lion, H. Pick, T. Gong, Z. Chen, P. Yang, L. T. Lovey and H. H. Girault, *Chem. Sci.*, 2016, **7**, 2987–2995.
38 S. L. Stott, C.-H. Hsu, D. I. Tsukrov, M. Yu, D. T. Miyamoto, B. A. Waltman, S. M. Rothenberg, A. M. Shah, M. E. Smas, G. K. Korir, F. P. Floyd Jr., A. J. Gilman, J. B. Lord, D. Winokur, S. Springer, D. Irimia, S. Nagrath, L. V. Sequist, R. J. Lee, K. J. Isselbacher, S. Maheswaran, D. A. Haber and M. Toner, *Proc. Natl. Acad. Sci. U. S. A.*, 2010, **107**, 18392–18397.
39 P. Zhang, X. Zhou, M. He, Y. Shang, A. L. Tetlow, A. K. Godwin and Y. Zeng, *Nat. Biomed. Eng.*, 2019, **3**, 438–451.
40 S. Wang, K. Liu, J. Liu, Z. T. F. Yu, X. Xu, L. Zhao, T. Lee, E. K. Lee, J. Reiss, Y.-K. Lee, L. W. K. Chung, J. Huang, M. Rettig, D. Seligson, K. N. Duraiswamy, C. K. F. Shen and H.-R. Tseng, *Angew. Chem., Int. Ed.*, 2011, **50**, 3084–3088.
41 R. H. Liu, M. A. Stremler, K. V. Sharp, M. G. Olsen, J. G. Santiago, R. J. Adrian, H. Aref and D. J. Beebe, *J. Microelectromech. Syst.*, 2000, **9**, 190–197.
42 H. Yuan, Z. Liu, L. Liu, F. Lv, Y. Wang and S. Wang, *Adv. Mater.*, 2014, **26**, 4333–4338.
43 J. Zhang, R. Oueslati, C. Cheng, L. Zhao, J. Chen, R. Almeida and J. Wu, *Biosens. Bioelectron.*, 2018, **112**, 48–53.
44 W. Wang, L. Liu, S. Song, L. Xu, H. Kuang, J. Zhu and C. Xu, *Sci. China Mater.*, 2016, **59**, 665–674.
45 Y. Li, J. Zhu, H. Zhang, W. Liu, J. Ge, J. Wu and P. Wang, *Sens. Actuators, B*, 2018, **259**, 492–497.
46 T. Lee, J. Lim, K. Park, E.-K. Lim and J.-J. Lee, *ACS Sens.*, 2020, **5**, 3099–3108.
47 B. K. Hubbard and C. T. Walsh, *Angew. Chem., Int. Ed.*, 2003, **42**, 730–765.
48 C. Walsh, *Science*, 1999, **284**, 442–443.
49 S. Manikandan, S. Ganesapandian, M. Singh and A. K. Kumaraguru, *Curr. Res. Bacteriol.*, 2011, **4**, 9–15.
50 A. Piette and G. Verschraegen, *Vet. Microbiol.*, 2009, **134**, 45–54.
51 A. C. Gales, H. S. Sader, R. N. Jones and S. P. Grp, *Diagn. Microbiol. Infect. Dis.*, 2002, **44**, 289–299.
52 A. M. Ferreira, M. F. Bonesso, A. L. Mondelli and M. de Lourdes Ribeiro de Souza da Cunha, *J. Microbiol. Methods*, 2012, **91**, 406–411.
53 G. Bonkat, R. Bartoletti, F. Bruyére, T. Cai, S. E. Geerlings, B. Köves, S. Schubert and F. Wagenlehner, *European Association of Urology Guidelines*, European Association of Urology Guidelines Office, Arnhem, The Netherlands, 2020 edn, 2020, vol. presented at the EAU Annual Congress Amsterdam 2020.
54 C. A. Gaydos and T. C. Quinn, *Curr. Opin. Infect. Dis.*, 2005, **18**, 55–66.
55 M. Medeiros, V. K. Sharma, R. Ding, K. Yamaji, B. Li, T. Muthukumar, S. Valderde-Rosas, A. M. Hernandez, R. Munoz and M. Suthanthiran, *J. Immunol. Methods*, 2003, **279**, 135–142.